Dendrite Development Regulated by CREST, a Calcium-Regulated Transcriptional Activator

Hiroyuki Aizawa,* Shu-Ching Hu,* Kathryn Bobb, Karthik Balakrishnan, Gulayse Ince, Inga Gurevich, Mitra Cowan, Anirvan Ghosh†‡

The lasting effects of neuronal activity on brain development involve calcium-dependent gene expression. Using a strategy called transactivator trap, we cloned a calcium-responsive transactivator called CREST (for calcium-responsive transactivator). CREST is a SYT-related nuclear protein that interacts with adenosine 3′,5′-monophosphate (cAMP) response element–binding protein (CREB)–binding protein (CBP) and is expressed in the developing brain. Mice that have a targeted disruption of the *crest* gene are viable but display defects in cortical and hippocampal dendrite development. Cortical neurons from *crest* mutant mice are compromised in calcium-dependent dendritic growth. Thus, calcium activation of CREST-mediated transcription helps regulate neuronal morphogenesis.

Neuronal activity influences many aspects of central nervous system development, including cell survival, axonal and dendritic remodeling, and synaptic plasticity (*1*). Most of these effects are mediated by calcium signaling (*2*). The acute effects of calcium influx, such as the rapid change in synaptic transmission that accompanies synaptic plasticity, are mediated by posttranslational modifications of proteins that are already present in the cell. In contrast, many of the long-term effects of calcium signaling, such as activity-dependent dendritic growth, long-term plasticity in sensory systems, and memory consolidation, involve calcium-dependent transcription (*2*–*4*). To identify calcium-regulated transcription factors in cortical neurons, we developed a new strategy called transactivator trap. Here, we describe the cloning and functional characterization of one of these genes, called CREST. CREST is a CBP-interacting protein that plays a central role in regulating development of cortical dendrites.

Transactivator trap: A strategy to clone calcium-activated transcription factors. Transactivator trap takes advantage of the modular nature of transcription factors in that their transactivation domain can often function separately from their DNA binding domains (DBDs) (*5*, *6*). For example, transactivation domains fused to the DBD of the yeast GAL4 transcription factor can induce expression of a reporter gene driven by the yeast upstream activating sequence (UAS) (*7*, *8*). We reasoned that if we generated a cDNA library in which cDNAs were fused to the GAL4 DBD and transfected pools of this GAL4-cDNA library along with a UAS-driven reporter gene into neurons, then the GAL4-cDNA plasmids should be translated as fusion proteins in the transfected cell and targeted to the UAS site of the reporter. Under most conditions, we would not expect any reporter activity, because most cDNAs do not encode transcription factors. However, if the cDNA that is fused to GAL4 encodes a calcium-activated transcription factor, then there should be no reporter activity in unstimulated cells, but the reporter should be expressed after calcium stimulation (Fig. 1, A and B).

To identify calcium-regulated transcription factors expressed in the developing brain, we generated a GAL4-cDNA library from the cerebral cortex of postnatal day 1 (P1) rats (*7*, *8*). We screened 200 pools of 1000 cDNA each by transfecting them along with the UAS–chloramphenicol acetyltransferase (CAT) reporter into duplicate wells containing embryonic day 18 (E18) rat cortical neurons at 3 to 5 days in vitro (DIV) (*9*, *10*). In the absence of stimulation, virtually all pools were devoid of expression of the CAT reporter. After depolarization by KCl, which induces calcium influx through voltage-sensitive calcium channels (VSCCs), 15 pools showed strong calcium inducibility (Fig. 1, A to C). Each of these pools is predicted to contain at least one cDNA that encodes a putative calcium-induced transactivator. The fact that we found very few CAT-positive cells in unstimulated cultures (although the li-

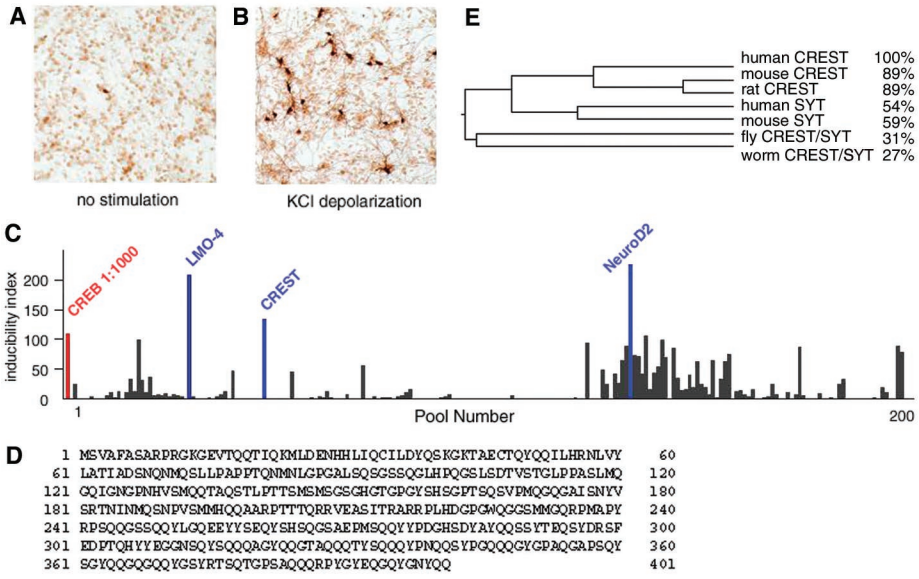

Fig. 1. Use of transactivator trap to clone *crest*. (**A** and **B**) Example of CAT immunoreactivity in unstimulated and stimulated E18 cortical cultures in a positive pool from this screen. (**C**) Summary of results from the primary screen to identify calcium-regulated transcription factors in cortical neurons. The inducibility index is the ratio of the number of CAT-positive cells in stimulated and unstimulated wells. The positive control (red) is GAL4-CREB diluted with GAL4-DBD at a ratio of 1:1000. The pools that yielded LMO-4, CREST, and NeuroD2 are indicated in blue. (**D**) Sequence of mammalian CREST protein (GenBank accession number AY034073). (**E**) Phylogenic tree deduced from an alignment of different members of the CREST/SYT family with the MegAlign program (*26*).

Department of Neuroscience, Johns Hopkins University School of Medicine, Baltimore, MD 21205, USA.

*These authors contributed equally to this work.
†Present address: Division of Biology, University of California, San Diego, 9500 Gilman Drive, La Jolla, CA 92093, USA.
‡To whom correspondence should be addressed. E-mail: aghosh@ucsd.edu

brary must contain some basal or constitutively active transcription factors) probably reflects the fact that at high dilutions only strong transactivators are able to drive sufficient CAT expression for detection.

We used two methods to reduce these pools to single cDNAs. In the first method, a positive pool was divided into smaller pools and transfected with the UAS-CAT reporter into cortical neurons for a second round of screening. This process was repeated until a single cDNA was identified. In the second method, a positive pool from the first round of screening was transfected along with the UAS–yellow fluorescent protein (YFP) reporter for a second round of screening. After stimulation, individual YFP-positive cells were retrieved with a micropipette. DNA isolated from these cells was directly transformed into bacteria, and plasmid DNA from individual bacterial clones was tested for transactivation. So far, we have used the transactivator trap approach to identify four genes that encode putative calcium-regulated transactivators. They include a basic helix-loop-helix protein (Neuro-D2), two *Lin*-11 *Isl*-1 *Mec*-3 proteins (LMO-2 and LMO-4), and a previously unknown protein related to the transcription coactivator SYT (*11*). Here, we describe the characterization of the SYT-related protein, CREST.

Characterization of the *crest* gene and CREST-mediated transcription. The *crest* transcript has an estimated size of 4.5 kb and contains an open reading frame of 1206 base pairs that begins with the first methionine codon within a Kozak consensus sequence and is followed by a polyadenylation signal at the end. This open reading frame encodes a 402–amino acid protein, which is most homologous (54% amino acid identity) to the SYT proto-oncogene (Fig. 1D). Mutations in SYT, which is a transcription coactivator, are linked to the occurrence of synovial sarcoma (*11–14*). SYT interacts with p300 and has been implicated in the control of cell adhesion (*15*). Sequence comparison with SYT indicates that CREST has an N-terminal autoregulatory domain, an internal methionine-rich region thought to be involved in protein-protein interaction, and a C-terminal transactivation domain (fig. S1). We have identified members of the CREST/SYT family in the worm, fly, rodent, and human (Fig. 1E).

We examined the calcium dependence of CREST-mediated transcription by transfecting cortical neurons with GAL4-CREST and UAS-CAT and stimulating cells under different conditions. The cultures were depolarized with increased extracellular KCl (to activate VSCCs) or stimulated with glutamate to induce calcium influx. Depolarization-induced CREST-mediated transcription was largely inhibited by the VSCC blocker nifedipine and by the calcium chelater EGTA but not by the *N*-methyl-D-aspartate (NMDA) antagonist D,L-2-amino-5-phosphonovaleric acid (APV) (Fig. 2A), indicating that membrane depolarization leads to CREST-mediated transcription by calcium influx by means of VSCCs. Stimulation with the neurotransmitter glutamate also induced CREST-mediated transcription. Glutamate-induced transcription was inhibited by APV and EGTA but not by nifedipine, suggesting that calcium influx by means of NMDA receptors is required for glutamate-induced CREST-mediated transcription (Fig. 2A). These observations indicate that calcium influx by means of VSCCs as well as NMDA receptors can induce CREST-mediated transcription.

To identify the domains of CREST that contribute to calcium-responsiveness, we examined the effects of various deletions on CREST-mediated transcription (Fig. 2B). N-terminal deletions in GAL4-CREST

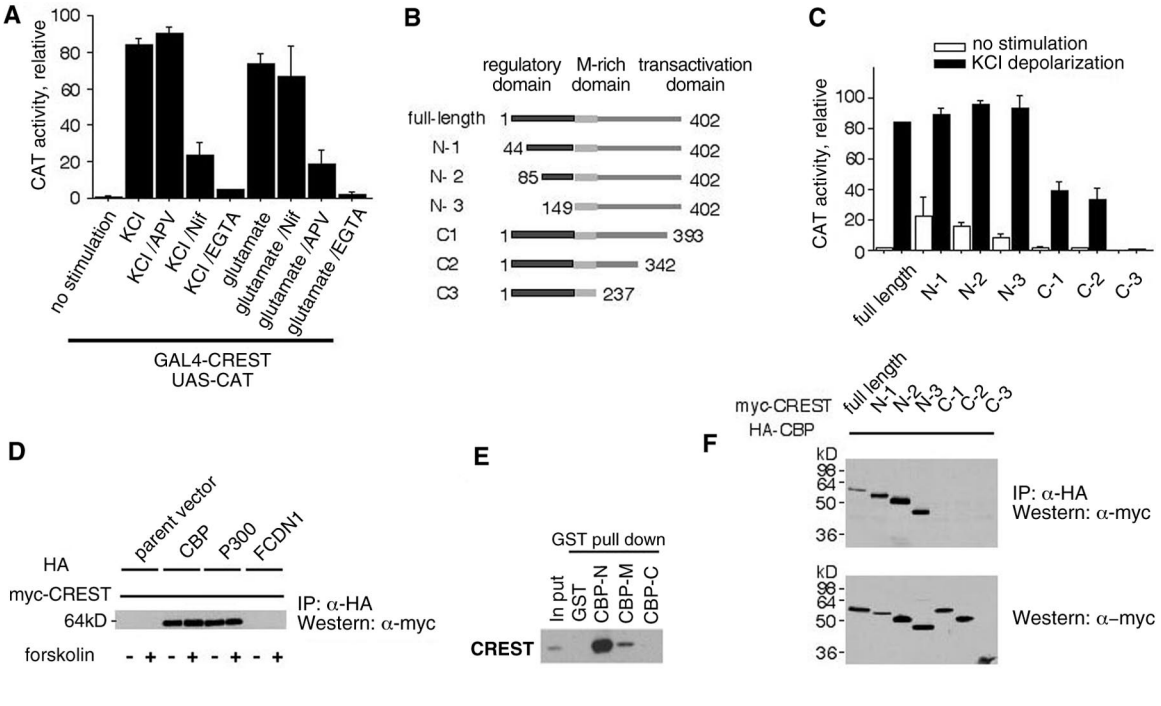

Fig. 2. Properties of CREST-mediated transcription and interaction with CBP. (**A**) Relative CAT activity in E18 cortical neurons transfected with GAL4-CREST and UAS-CAT at 3 DIV, and stimulated as indicated at 5 DIV (50 mM KCl, 20 μM nifedipine, 200 μM APV, 2 mM EGTA, and 100 μM glutamate). (**B**) Schematic representation of serial deletion fragments of CREST used to map the domains of CREST that contribute to calcium-dependent transactivation. M-rich, methionine-rich. (**C**) Relative CAT activity in E18 cortical neurons transfected at 3 DIV with a UAS-CAT together with each of the GAL4-fused deletion constructs of CREST, and stimulated at 5 DIV as indicated. The fold induction (indicated in parentheses) of each of the deletion constructs shown in (B) was as follows: full-length (85X), N1(3.9X), N2(6X), N3(10X), C1(35X), C2(33X), and C3(1X). (**D**) Immunoprecipitation of CREST with CBP and p300. Human embryonic kidney (HEK) 293 cells were transfected with Myc-CREST and one of these HA-tagged constructs: HA-parent vector, HA-CBP, HA-p300, or HA-FCDN1 [Full-length cytoplasmic domain of Notch-1, used as a negative control (*27*)]. Cells were stimulated as indicated, lysed, and immunoprecipitated with an antibody to HA. The immunoprecipitates were resolved by SDS-PAGE, and the Western blot was probed with an antibody to Myc. (**E**) Direct binding assay of CREST to CBP in vitro. T7-tagged $(His)_6$-CREST was expressed in bacterial cells and purified using Ni^{2+}–nitrilotriacetic acid (NTA) agarose. GST, GST-CBP–N terminus, GST-CBP-middle, GST-CBP–C terminus, and GST-CREST proteins were expressed in bacterial cells, purified, and immobilized onto glutathione beads. T7-tagged protein was mixed with GST-fusion protein beads at room temperature for 20 min, and bound protein was analyzed by Western blotting with an antibody to T7. (**F**) N terminus of CREST binds to CBP. HEK 293 cells were transfected with HA-CBP along with Myc-tagged CREST deletion constructs (B), and immunoprecipitated with an antibody to HA. The HA immunoprecipitates were separated by SDS-PAGE and probed with an antibody to Myc (upper blot). Similar amounts of input Myc-tagged proteins in each sample were confirmed by probing with an antibody to Myc (lower blot).

led to an increase in transactivation in unstimulated neurons but did not affect the level of transactivation seen after stimulation (Fig. 2C). In contrast, C-terminal deletions did not affect transactivation in unstimulated cells but markedly attenuated calcium-induced transactivation. A deletion of the last nine amino acids (393 to 402) led to a 50% decrease in depolarization-induced transactivation, whereas a deletion that removed the last 135 amino acids completely abolished inducible transactivation. Therefore, both the N- and C-terminal domains contribute to CREST-mediated transcription; the N-terminal domain is required for suppressing transactivation in the basal state, and the C-terminal domain is required for calcium-induced transactivation.

Association of CREST with CBP. The CREST-related protein SYT has been reported to interact with the histone acetyl transferase p300 (*15*). To determine whether CREST could also interact with p300, or the p300-related protein CBP (*16*–*19*), we transfected 293 cells with tagged proteins. Myc-CREST could be co-precipitated with both CBP and p300 (Fig. 2D). In vitro pulldown assays with purified bacterially expressed T7-CREST and glutathione *S*-transferase (GST)–CBP indicated that CREST can directly bind to CBP (Fig. 2E). Deletion analysis indicated that CREST binds to the N terminus of CBP (Fig. 2F).

To identify the domain of CREST that mediates the interaction with CBP, we cloned CREST deletion constructs into the Myc-PRK5 vector (Fig. 2B). Each of the constructs was transfected into 293 cells together with hemagglutinin (HA)–tagged CBP. Immunoprecipitation with anti-HA followed by anti-Myc Western blots revealed that N-terminal deletions have no effect, but the deletion of only nine amino acids at the C terminus of CREST abolishes association with CBP (Fig. 2F). Thus, the C terminus of CREST acts as a CBP-binding domain. The C terminus deletion reduces calcium-induced transactivation by 50% (Fig. 2C), suggesting that the interaction with CBP contributes to CREST-mediated transcription.

Expression of CREST in the developing brain. To identify regions of the brain where CREST may function, we examined the expression of CREST with Northern blot and in situ hybridization analysis. Northern blot analysis of different adult rat tissues indicated that the expression of CREST is relatively enriched in the brain but is also present in the heart, liver, kidney, and testis (Fig. 3A). In the developing cerebral cortex, *crest* message is detected as early as E18, and expression reaches its peak at P1, declines after P10, and remains at a relatively low level throughout adulthood (Fig. 3B). In situ hybridization studies

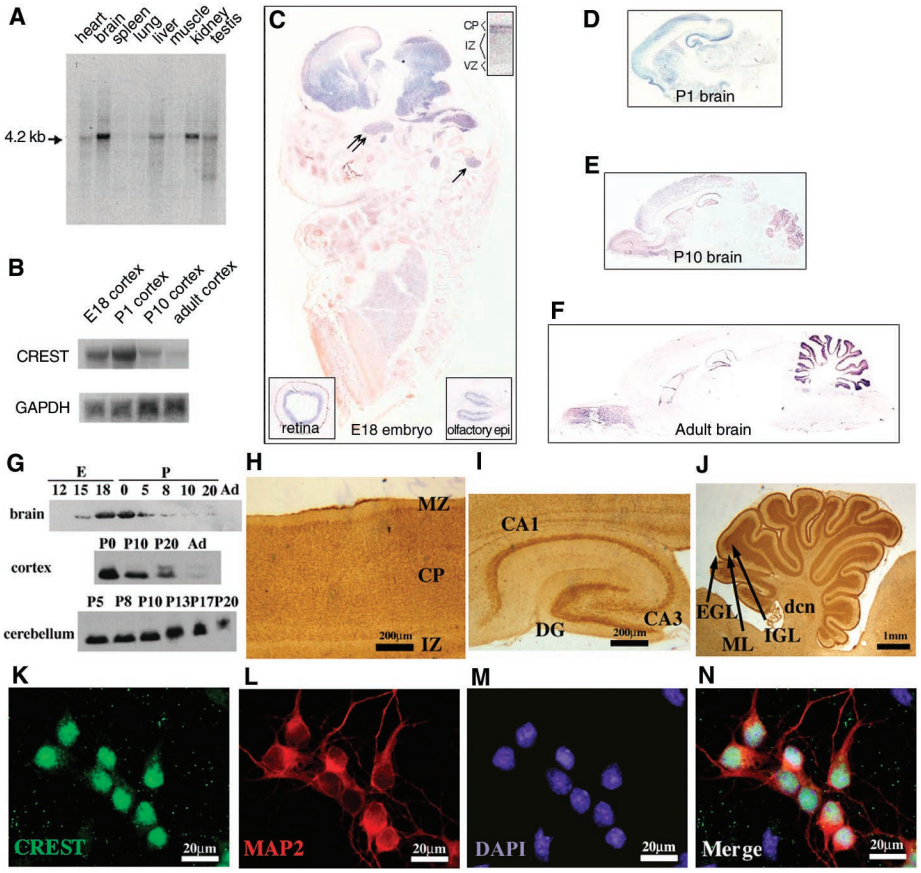

Fig. 3. Developmental expression of *crest* mRNA and CREST protein. (**A**) Northern blot of mRNA harvested from different adult rat tissues, hybridized with a full-length probe directed against *crest* coding sequence. (**B**) Northern blot of mRNA isolated from the cortex at different developmental ages hybridized with a *crest* probe. The same blot was subsequently stripped and hybridized with a glyceraldehyde-3-phosphate dehydrogenase probe (loading control). (**C** to **F**) In situ hybridization analysis of *crest* expression in the rat nervous system at indicated ages, presented in sagittal sections. CP, cortical plate; IZ, intermediate zone; VZ, ventricular zone. No signal was detected in sections hybridized with the sense control. (**G**) Western blotting of protein extracts from indicated regions using antibody to CREST. E, embryonic age; P, postnatal age. Equivalent protein loading was confirmed by probing the same blots with a β-actin antibody. (**H** to **J**) Immunohistochemistry of P10 sagittal sections of the cerebral cortex (H), hippocampus (I), and cerebellum (J) treated with the antibody to CREST (*28*). MZ, marginal zone; DG, dentate gyrus; EGL, external granule layer; IGL, internal granule layer; ML, molecular layer; dcn, deep cerebellar nuclei. Scale bars, 200 μm [(H) and (I)] and 1 mm (J). (**K** to **N**) Subcellular localization of CREST in E18 cortical cultures visualized by immunofluorescence with antibodies to CREST and MAP2. Nuclei are labeled with 4′,6′-diamidino-2-phenylindole. Scale bars, 20 μm.

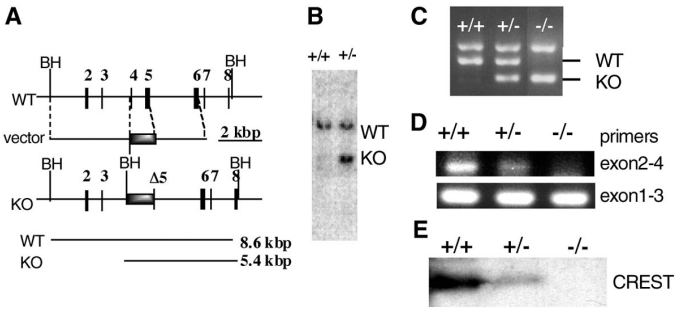

Fig. 4. Targeted disruption of the *crest* locus. (**A**) Targeting strategy (*29*). The genomic organization of the *crest* locus is shown on top. Vertical bars represent exons 2 to 8 of the *crest* gene. The second line shows the targeting vector. A thick bar represents neomycin minigene cassette, which replaces exon 4 and a part of exon 5. The third line shows the predicted genomic structure of the recombined allele. The predicted sizes of BamHI (BH) digestion fragments from the wild-type (WT) and targeted (KO) allele is shown. kbp, kilobase pairs. (**B**) Genomic Southern blotting of wild type (+/+) and homologously recombined (+/–) ES cells. (**C**) PCR genotyping of wild-type (+/+), heterozygote (+/–), and homozygote (–/–) mice. (**D**) RT-PCR analysis of mRNA from mice of indicated genotypes using primers that span exons 1 to 3 or exons 2 to 4. (**E**) Western blotting of total brain proteins with the antibody to CREST.

revealed that at E18 *crest* mRNA is expressed in the forebrain, midbrain, and hindbrain (Fig. 3C). Within the forebrain, *crest* is expressed in postmitotic cells of the cortical plate, and not in proliferating neuroblasts in the ventricular zone (Fig. 3C). At this stage, *crest* mRNA could also be detected in other structures of central and peripheral nervous systems, including the trigeminal ganglion, superior cervical ganglion, retina, and olfactory epithelium (Fig. 3C) (*20*). Within the brain, *crest* expression decreases through development but continues to be expressed at high levels in the olfactory bulb, hippocampus, and cerebellum into adulthood (Fig. 3, D to F).

To investigate the distribution of CREST protein in the brain, we generated polyclonal antibodies to a full-length CREST protein. In rat brain extracts, this antibody recognizes a single band at about 55 kD, which comigrates with recombinant CREST expressed in 293T cells (Fig. 3G). Consistent with the Northern blot analysis, Western blots of whole-brain extracts indicate that CREST expression is developmentally regulated (Fig. 3G). Expression in the cortex is high at birth and declines substantially by P20 (Fig. 3G). Immunohistological analysis showed that at P7 CREST is expressed in all cortical layers, and in the hippocampus, expression is high in the cell body layers of all subdivisions (Fig. 3, H and I). In the cerebellum, expression is restricted to the internal and external granule layers, indicating that CREST is expressed principally by granule cells (Fig. 3J). Immunofluorescence analysis of E18 cortical cultures at 5 DIV indicated that

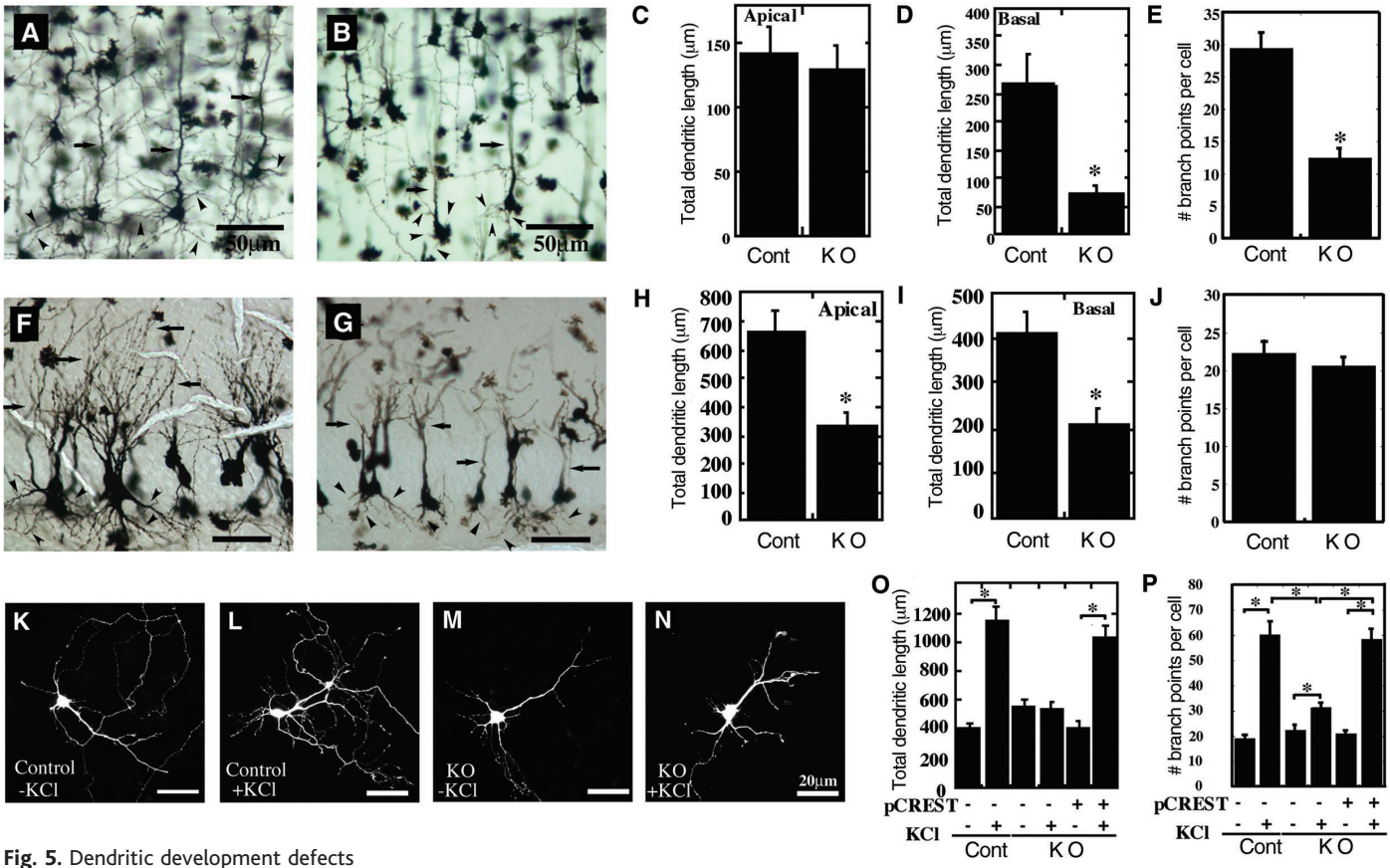

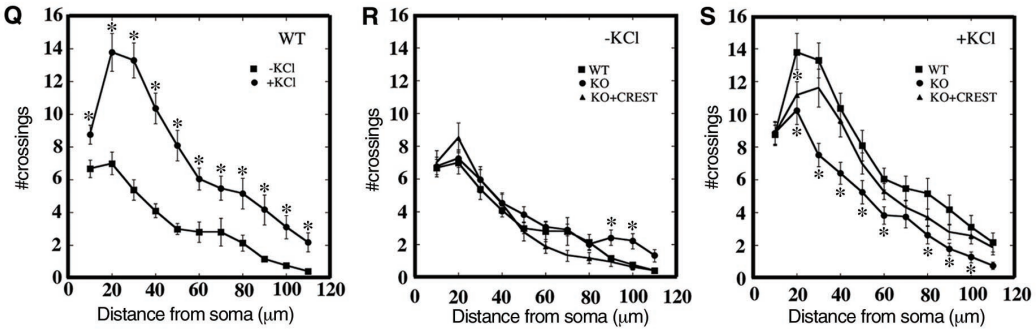

Fig. 5. Dendritic development defects in *crest* mutant mice. (**A** and **B**) Golgi staining of cerebral cortex in control (A) and *crest* mutant (B) mice. The apical dendrites are oriented toward the top of the figure. Arrows show apical dendrites. Arrowheads show basal dendrites. (**C** to **E**) Quantitative analysis of apical (C) and basal (D) dendrites and total branch points (E) in cortical layer 5 pyramidal neurons in control (Cont) and *crest* mutant (KO) mice. (**F** and **G**) Golgi staining of pyramidal neurons of hippocampus CA3 region in control (E) and *crest* mutant (F) mice. (**H** to **J**) Quantitative analysis of apical (H) and basal (I) dendrites, and total branch points (J) in hippocampal CA3 pyramidal neurons in control and *crest* mutant mice. (**K** to **N**) Examples of GFP-transfected cortical neurons from E18 wild-type and *crest* mutant mice cultured for 5 days and stimulated overnight with 50 mM KCl where indicated. (**O** and **P**) Quantification of total dendritic length and branch points in cortical neurons from E18 wild-type and *crest* mutant mice cultured for 5 days and stimulated overnight with 50 mM KCl where indicated. *Crest* null cultures transfected with a *crest* plasmid are indicated as pCREST+. (**Q** to **S**) Sholl analysis of dendritic branch distribution in neurons cultured from wild-type (WT) or *crest* mutant (KO) mice, stimulated as indicated. *Crest* null neurons transfected with a *crest* plasmid are indicated as KO+CREST. *, $P < 0.05$ [compared with –KCL in (Q); compared with the wild type in (R) and (S)].

CREST is a nuclear protein (Fig. 3, K to N). The localization was not notably altered by calcium influx (fig. S3).

Functional analysis of CREST through gene targeting. The expression pattern and calcium activation properties of CREST suggest that it is likely to be involved in regulating aspects of nervous system development. To identify the specific function of CREST in vivo, we generated mice that have a targeted disruption of the *crest* gene. In the targeting vector we eliminated exon 4 and part of exon 5 to eliminate the transactivation domain (Fig. 4A). Even if an alternate message were generated by skipping exons 4 and 5, sequences downstream of exon 5 would be frame-shifted to create a nonsense mutation. To generate *crest* knockout mice, transfected embryonic stem (ES) cells were screened for homologous recombination by Southern blotting. Correctly targeted ES cell clones were used to generate chimeras, which were used in subsequent crosses to obtain homozygous mutant mice (Fig. 4, B and C).

To evaluate the effect of gene targeting on *crest* expression, we carried out reverse transcription polymerase chain reaction (RT-PCR) and Western blot analysis on cortical extracts. RT-PCR with exon-specific primers revealed the presence of RNA that contained exons 1 and 3 but not exon 4 (Fig. 4D). Western blot analysis showed that there is no detectable full-length or truncated CREST protein in homozygous targeted mice (Fig. 4E) (*20*). The homozygous *crest* mutant mice are therefore likely to be null, although it is difficult to formally rule out the possibility that a short N-terminal fragment is expressed (encoded by exons 2 and 3, about 5 kD) below detection limits.

crest mutant mice are born in expected Mendelian ratio and are indistinguishable from littermates at birth. As they develop further, *crest* mutant mice are somewhat smaller than littermates and show coordination defects. There is increased mortality in *crest* mutant mice beginning at about P14, and about 80% of the mutants die by P28. Less than 20% of *crest* mutants survive to adulthood, and they are infertile.

Immunofluorescence analysis of cortical sections from wild-type and *crest* mutant mice with antibodies to neuronal protein [microtubule-associated protein 2 (MAP2), NeuN] and glial fibrillary acidic protein (GFAP) revealed no qualitative differences in the expression of neuronal and glial antigens in mice of the two genotypes (fig. S2). Terminal deoxynucleotidyl transferase–mediated deoxyuridine triphosphate nick end labeling staining did not reveal substantial differences between control and *crest* mutant animals, suggesting that the lack of CREST does not lead to a substantial increase in cell death (fig. S2). The main difference between wild-type and *crest* mutant brains was that the overall size of the cortex and cerebellum was reduced in *crest* mutant mice (fig. S2).

Much of the growth of the brain during the early postnatal period reflects increases in dendritic arborization, which is regulated in part by calcium-dependent transcription (*21*). Dendritic growth and branching was greatly compromised in the *crest* mutant mice that were analyzed at P7 (Fig. 5, A to J). Although the orientation of apical dendrites was unaffected, the total dendritic length in both cortical layer 5 and hippocampal CA3 neurons was reduced by between 50 and 80%. There was also a marked decrease in dendritic branching in cortical neurons from *crest* mutant mice (Fig. 5E). Thus, one of the main consequences of the loss of CREST function is decreased dendritic growth and branching.

To determine if CREST function was necessary for calcium-induced dendritic growth, we examined whether depolarization-induced dendritic growth was compromised in *crest* mutant cells. *crest* mutant cells in culture had well-differentiated dendrites, and the total dendritic length was comparable between wild-type and *crest* mutant cells in unstimulated cultures. Depolarization induced a robust increase in dendritic length in control neurons but not in *crest* mutant neurons (Fig. 5, K to O). Depolarization-induced dendritic growth could be restored in *crest* mutant mice by transfecting a full-length *crest* plasmid, indicating that *crest* can act cell autonomously to regulate dendritic growth (Fig. 5O). Branch point analysis and Sholl analysis also revealed defects in depolarization-induced branching in cortical neurons from *crest* mutant mice (Fig. 5, P to S). These, too, could be rescued by transfecting *crest* cDNA. Thus, CREST function is required for calcium-dependent dendritic growth and branching in cortical neurons.

Discussion. The transactivator trap screen can be used to clone transcriptional activators regulated by any extracellular or intracellular signal. We used the screen to clone several calcium-activated transactivators in cortical neurons, including CREST. Although the mechanism by which CREST regulates transcription is not known, the interaction with CBP is of interest given previous studies implicating CBP in calcium-dependent transcription (*22–24*). We have also found that CREST interacts with the chromatin remodeling proteins BAF250 and BRG-1 (*25*). These interactions suggest that the CREST complex may regulate transcription by means of calcium-dependent modification of chromatin structure. Because CBP is known to interact with several DNA binding proteins, it is possible that the CREST-CBP-BAG250/BRG-1 complex gets recruited to specific promoters by CBP.

Our experiments suggest that activation of CREST is part of the mechanisms by which calcium signaling regulates dendritic development during early postnatal development. We have previously shown that CREB function is required for calcium-induced dendritic growth (*21*), and the present findings provide further evidence for the involvement of calcium-regulated transcription in regulating dendritic development. We find that calcium influx by means of NMDA receptors as well as VSCCs can activate CREST-mediated transcription, suggesting that CREST-mediated transcription can be regulated by synaptic activity. Although neurons are active throughout life, patterns of activity are coupled to growth control only during certain times in development. The transient expression of CREST in the cortex may provide a mechanism to couple activity to growth control only during certain developmental periods. In tissues, such as the hippocampus, where CREST continues to be expressed in the adult, the protein may serve a different function. Given the requirement for gene expression in many forms of plasticity, it is possible that CREST-dependent transcription also contributes to learning and memory.

References and Notes

1. L. C. Katz, C. J. Shatz, *Science* **274**, 1133 (1996).
2. A. Ghosh, M. E. Greenberg, *Science* **268**, 239 (1995).
3. E. Nedivi, *J. Neurobiol.* **41**, 135 (1999).
4. A. E. West *et al*., *Proc. Natl. Acad. Sci. U.S.A.* **98**, 11024 (2001).
5. L. Keegan, G. Gill, M. Ptashne, *Science* **231**, 699 (1986).
6. M. Ptashne, *A Genetic Switch* (Blackwell Scientific Publications and Cell Press, Cambridge, MA, 1992).
7. To determine the cDNA pool size appropriate for the screen, we used GAL4-CREB as a positive control in sequential dilution experiments. GAL4-CREB could induce detectable transactivation of UAS-CAT in the presence of competing GAL4-DBD at a ratio of 1:1000, suggesting a pool size of 1000 cDNAs.
8. The library is maintained in the form of 200 pools of 1000 cDNAs, as plasmid DNA as well as bacterial transformants.
9. Cultures were transfected at 3 DIV and stimulated by depolarization with 50 mM KCl overnight at 5 DIV. GAL4-CREB, diluted at 1:1000 with GAL4-DBD served as a positive control.
10. Materials and methods are available as supporting material on *Science* Online.
11. J. Clark *et al*., *Nature Genet.* **7**, 502 (1994).
12. N. R. dos Santos *et al*., *Hum. Mol. Genet.* **6**, 1549 (1997).
13. D. Brett *et al*., *Hum. Mol. Genet.* **6**, 1559 (1997).
14. C. Thaete *et al*., *Hum. Mol. Genet.* **8**, 585 (1999).
15. J. E. Eid, A. L. Kung, R. Scully, D. M. Livingston, *Cell* **102**, 839 (2000).
16. R. Kwok *et al*., *Nature* **370**, 223 (1994).
17. J. R. Lundblad, R. P. S. Kwok, M. E. Laurance, M. L. Harter, R. H. Goodman, *Nature* **374**, 85 (1995).
18. X. Yang, V. V. Ogryzko, J. Nishikawa, B. H. Howard, Y. Nakatani, *Nature* **382**, 319 (1996).
19. A. J. Bannister, T. Kouzarides, *Nature* **384**, 641 (1996).
20. H. Aizawa *et al*., data not shown.
21. L. Redmond, A. Kashani, A. Ghosh, *Neuron* **34**, 999 (2002).
22. S. Chawla, G. E. Hardingham, D. R. Quinn, H. Bading, *Science* **281**, 1505 (1998).
23. G. E. Hardingham, S. Chawla, F. H. Cruzalegui, H. Bading, *Neuron* **22**, 789 (1999).
24. S.-C. Hu, J. Chrivia, A. Ghosh, *Neuron* **22**, 799 (1999).
25. S.-C. Hu, H. Aizawa, A. Ghosh, unpublished results.

26. MegAlign program, DNASTAR, Madison, WI.
27. L. Redmond, S.-R. Oh, C. Hicks, G. Weinmaster, A. Ghosh, *Nature Neurosci.* **3**, 30 (2000).
28. To create the CREST antibody, We used PCR to amplify full-length *crest* cDNA from P0 mouse brain total RNA and cloned it into pET21 vector for expression of His-tagged CREST protein in bacteria. After isopropyl-β-D-thiogalactopyranoside induction, CREST protein was mainly collected in the inclusion body of the bacteria and extracted with 6 M urea. We further purified the protein with Ni-NTA agarose fractionation. After SDS–polyacrylamide gel electrophoresis (PAGE), the Coomassie brilliant blue–stained CREST band was excised and injected into rabbits to produce anti-CREST antiserum.
29. To generate the *crest* knockout mice, *crest* genomic DNA was cloned by screening a 129SVJ mouse genomic phage library (gift of A. Kolodkin) with full-length mouse *crest* cDNA as a probe. After mapping the restriction enzyme sites, we generated a knockout vector with a Neo gene cassette (Fig. 4). We deleted the poly(A) addition signal from the Neo gene cassette for poly(A) trapping method of gene targeting. The cassette replaced all of exon 4 and a 5′ portion of exon 5. ES cells transfected with the targeting vector and resistant to G418 and gancyclovir were expanded and screened by genomic Southern blotting. Correctly targeted ES cells were injected into C57B6J-derived blastocysts and resulted in the generation of several high-percentage chimeras, which produced germline targeted offspring. Genotyping of mice was performed on tail clip DNA by PCR.
30. We thank D. Livingston for the UAS-CAT construct; A. Lanahan for advice on library construction; A. Kolodkin for rat phage libraries; L. Redmond, A. Datwani, K. Whitford, M.-R. Song, and G. Ince for various procedures; J. Nathans, C. Montell, D. Ginty, P. Worley, S. Snyder, D. Linden, D. Murphy, P. Kim, M. Molliver for discussions; and M. Greenberg, D. Ginty, A. Kolodkin, and S. Snyder for comments on the manuscript. Supported by grants from NIH (MH60598 and NS39993), the March of Dimes Birth Defects Foundation (A.G.), the Klingenstein Foundation (A.G.), and a Merck Scholar Award (A.G.). H.A. was supported by a Uehara Memorial Foundation Research Fellowship.

Supporting Online Material
www.sciencemag.org/cgi/content/full/303/5655/197/DC1
Materials and Methods
Figs. S1 to S3

30 July 2003; accepted 28 October 2003

^{14}C Activity and Global Carbon Cycle Changes over the Past 50,000 Years

K. Hughen,[1]* S. Lehman,[3] J. Southon,[4] J. Overpeck,[5,6] O. Marchal,[2] C. Herring,[1] J. Turnbull[3]

A series of ^{14}C measurements in Ocean Drilling Program cores from the tropical Cariaco Basin, which have been correlated to the annual-layer counted chronology for the Greenland Ice Sheet Project 2 (GISP2) ice core, provides a high-resolution calibration of the radiocarbon time scale back to 50,000 years before the present. Independent radiometric dating of events correlated to GISP2 suggests that the calibration is accurate. Reconstructed ^{14}C activities varied substantially during the last glacial period, including sharp peaks synchronous with the Laschamp and Mono Lake geomagnetic field intensity minimal and cosmogenic nuclide peaks in ice cores and marine sediments. Simulations with a geochemical box model suggest that much of the variability can be explained by geomagnetically modulated changes in ^{14}C production rate together with plausible changes in deep-ocean ventilation and the global carbon cycle during glaciation.

Radiocarbon age may deviate significantly from calendar age as a result of time-varying processes affecting ^{14}C production in the atmosphere, as well as the distribution of ^{14}C among the active global carbon reservoirs (*1*). To account for such changes, radiocarbon age determinations must be calibrated against independent estimates of calendar age, but existing calibration data sets often lack temporal range and/or resolution. The current standard calibration, Intcal98 (*2*), extends at high resolution back to just ~14,600 calendar years before the present (14.6 cal. ka B.P.) on the basis of annual tree rings (*3*) and varved (annually layered) marine sediments (*4*). Paired ^{14}C and U/Th ages on corals (*5*) provide additional calibration points back to ~40 cal. ka B.P., but at much lower resolution. Varved lake sediments (*6*), U/Th ages on speleothems (*7*) and lake sediments (*8*), and marine sediments correlated to Greenland ice core chronologies (*9*, *10*) have also been used to constrain calibration and initial ^{14}C activity [expressed as Δ^{14}C (*11*)] beyond the range of Intcal98. In many cases, these records suggest that extremely large and rapid shifts in Δ^{14}C have occurred; however, these records also show disagreements before ~25 cal. ka B.P. that are as large as the reconstructed anomalies. Thus, considerable uncertainty remains in calibrating the older half of the ^{14}C time scale. Here, we present a calibration and reconstruction of Δ^{14}C back to 50 cal. ka B.P. on the basis of the correlation of ^{14}C data from Cariaco Basin sediments with the annual-layer time scale of the GISP2 Greenland ice core (*12*). Similarity between reconstructed Δ^{14}C and variations in ^{14}C production rate estimated from independent paleomagnetic and geochronologic data suggests that the calibration and Δ^{14}C reconstruction are accurate despite the lack of in situ calendric age control.

[1]Department of Marine Chemistry and Geochemistry, [2]Department of Geology and Geophysics, Woods Hole Oceanographic Institution (WHOI), Woods Hole, MA 02543, USA. [3]Institute of Arctic and Alpine Research, University of Colorado, Boulder, CO 80309, USA. [4]Department of Earth System Science, University of California, Irvine, CA 92697, USA. [5]Department of Geosciences, [6]Institute for the Study of Planet Earth, University of Arizona, Tucson, AZ 85721, USA.

*To whom correspondence should be addressed. E-mail: khughen@whoi.edu

Our ^{14}C series (Fig. 1) is constructed from 280 accelerator mass spectrometry (AMS) ^{14}C measurements on planktonic foraminifera extracted from discrete sediment samples in holes 1002D and 1002E from Ocean Drilling Program (ODP) leg 165, site 1002, in the Cariaco Basin (10°42.73′N, 65°10.18′W, 893-m water depth). The results span a ^{14}C age range of 55 to 12 ka B.P. and complement 355 varve-age calibrated ^{14}C measurements for the interval from ~15 to 10 cal. ka B.P. based on our prior studies of nearby Cariaco Basin sediment piston cores (*4*, *13*). AMS ^{14}C target preparation and measurement was conducted at three different institutions: Center for Accelerator Mass Spectrometry at Lawrence Livermore National Laboratory (CAMS-LLNL) (n = 127), Laboratory for AMS Radiocarbon Preparation and Research at University of Colorado, Boulder, and National Ocean Sciences AMS at WHOI (NSRL-NOSAMS) (n = 118), and the Keck CCAMS Facility at University of California, Irvine (n = 35) (Fig. 1 and table S1) (*14*). A constant 420-year marine reservoir age correction (difference between ^{14}C ages of surface water and atmosphere) was applied to all ^{14}C ages, in accordance with prior studies demonstrating that the local Cariaco Basin reservoir age has varied little, even when climate conditions and forcings have changed dramatically (*14*).

The initial ^{14}C chronology for hole 1002D showed a large age reversal from 14 to 14.5 meters below the sea floor (mbsf) (Fig. 1), in association with the boundary between successive 10-m core sections. We therefore performed additional measurements across the equivalent interval in adjacent hole 1002E, which was drilled in offsetting fashion. Magnetic susceptibility records were used to identify the disturbed section in 1002D and to align the two holes (fig. S1). The ^{14}C dates for undisturbed sections in both holes agree closely, but results from hole 1002E do not display a large age reversal (Fig. 1, inset) and were thus used to bridge the disturbed section.

Calendar age chronology. Our prior studies of Cariaco Basin sediments made use of annual varve counts to compare timing of abrupt changes in upwelling proxies to calendrically